# Ultimate spatial resolution accessible with a miniature HTS coil and a new-generation 1.5 T body scanner

**M. Poirier-Quinot[1], O. Girard[1], E. Laistler[1,2], R-M. Dubuisson[1], J-C. Ginefri[1], and L. Darrasse[1]**

[1]U2R2M, UMR8081 Univ Paris-Sud/CNRS, Orsay-Bicêtre, France, [2]MR Center of Excellence, Center for Biomedical Engineering and Physics, Medical University of Vienna, Vienna, Austria

**Purpose:**

With the extensive development of ultrafast acquisition techniques such as EPI to explore brain and cardiac functions by MRI, the strong demand on the gradient system has led to a new generation of commercially available body scanners, now able to achieve amplitudes reaching 50 mT/m at switching speeds of a few 100 µs. At reduced spatial encoding speeds, such gradient performances are in principle sufficient to achieve nominal resolution much less than $10^{-3}$ mm$^3$ [1]. With earlier MRI systems, the adjunction of a small dedicated gradient was needed to achieve the so-called microscopic resolution [2]. However the effective spatial resolution with new-generation systems is still constrained by the limited SNR achievable at the current field strength of 1.5 T with conventional copper coils, even when calling to miniature surface coils with highest sensitivities and to acquisition times of several hours [1]. The present work investigates the spatial resolution performance accessible with a new-generation 1.5 T body scanner equipped with a home-made 13 mm surface coil made of high temperature superconductor (HTS) to improve sensitivity and achieve effective isotropic resolutions better than $10^{-5}$ mm$^3$. Comparison is provided with the coil of diameter 23 mm available from the manufacturer in a standard "microscopy" package.

**Materials and Methods:**

Experiments were performed on a 1.5 T Philips Achieva MR scanner, recently implemented in the CIERM facility in Bicêtre Hospital (France), featuring in "enhanced mode" a maximum gradient power of 66 mT/m at a rise time of 800 µs. In the present work gradient excursion was limited to 50 mT/m. Similarly to reference [3], the HTS coil consisted of 2 spiral-shaped windings of YbaCuO with a mean diameter of 13 mm, deposited on both sides of a sapphire wafer of thickness 330 µm. The coil, cooled at 77 K, offered an unloaded quality factor close to 8,000 when positioned at the centre of the MRI magnet. The coil was operated in received mode using the third-party input adapter (SMC) available from the manufacturer. The radiofrequency field B1 provided by the body coil was concentrated by a factor of about 300 times at close proximity to the HTS coil, accounting to the high quality factor moderated by non-linear effects at high B1 levels [4]. Flip angle adjustment was achieved by varying the pulse length and keeping the B1 amplitude constant.A test phantom was made of a capillary tube of 1 mm inner diameter filled with doped water (3 mM DOTA/Guerbet Research-France, $T_1$ /$T_2$ = 98/84 ms), containing a single hair (∅ of 95.9±0.3 µm) folded once to limit the risk of motion. MR phantom images were performed with a 3D gradient-echo RF-spoiled acquisition at different voxel size (isotropic) and matrix size. In any imaging protocol the flip angle was adjusted at Ernst's angle value to accommodate the TR/T1 ratio for best SNR performance. Asymmetric echo sampling (by about 62%) was systematically involved in order to get reduced echo times. However the absolute shortest TE values could only be achieved with rather long TR values, due to a limitation of the gradient duty cycle imposed by the MR system at the highest gradient amplitudes of 50 mT/m, actually reached by the phase-encoding gradient pulses. The implication was long acquisition times $t_{acq}$ and poor signal-averaging efficiency (SAE). The sequence parameters corresponding to the situation of absolute shortest TE for different isotropic spatial resolutions are referred to as Protocol 1 series. Defining SAE as the fraction of the acquisition time effectively used for echo sampling, it is given by 0.62/(BW*TR) where BW is the acquisition bandwidth expressed in Hz/pixel and the factor 0.62 accounts for echo sampling asymmetry. With the whole Protocol 1 series SAE was close to 0.056. Protocol 2 series was designed to increase SAE up to 0.62, the shortest TE being now imposed when reaching the 50 mT/m with the pre-phasing pulse of the readout gradient. All protocols were applied with a single average per phase-encoding step excepted for Protocol 1 with (20µm)$^3$ voxels involving 2 averages.

**Results**:

Parameters of Protocol 1 and Protocol 2 series are reported in Table1, with measured SNR values on the test phantom normalized by unit of acquisition time. Figure1 a and b shows images acquired with Protocol 1 and 2 at (20 µm)$^3$. The SNR is clearly sufficient to depict the actual resolution of 20 µm (the intensity-profile step into the phantom is achieved in 2 pixels). The hair thickness could be measured by MRI with an average accuracy of 5 µm. Background noise was found to be uniform along the frequency-encoding axis within a maximum amplitude deviation of less than 22% with Protocol 1-(40µm)$^3$, the one involving the largest acquisition bandwidth. Protocol 2-(40µm)$^3$ with 40 averages was also applied to the test phantom using the Philips 23 mm microscopy coil (Micro23) and the resulting image compared to the HTS coil image with the same protocol but single averaged (Figure 1 d and e). The measured SNR gain with the HTS coil compared to the Micro23 coil was about 31.7±1.7. This magnitude was consistent with scaling rules applying to small surface coils [5]. Finally, Protocol 2-(40µm)$^3$ was applied on a *Trivia monacha*, a small gastropod found on the Atlantic Coast filled with the 3 mM DOTA solution. Images of orthogonal orientations extracted from a 47 min. acquisition are shown Figure1. e and f.

| Protocols | *TR/TE* (ms) | Acq Matrix | *Bw* (Hz/pixel) | $t_{acq}$ (min) | $SNR/\sqrt{t_{acq}}$ |
|---|---|---|---|---|---|
| 1-(40µm)$^3$ | 129/10 | 256x256x100 | 85.2 | 18 | 4.4±0.1 |
| 1-(30µm)$^3$ | 170/12 | 256x256x134 | 63.0 | 31 | 1.8±0.03 |
| 1-(20µm)$^3$ | 248/17 | 256x256/200 | 42.6 | 135 | 0.53±0.02 |
| 2-(40µm)$^3$ | 77/18 | 256x256x100 | 8.6 | 10.5 | 10.9±0.2 |
| 2-(30µm)$^3$ | 101/23 | 256x256x134 | 10 | 14.6 | 5.1±0.1 |
| 2-(20µm)$^3$ | 143/35 | 256x256/200 | 7 | 39 | 1.31±0.03 |

Table 1 : Sequence parameters and SNR measures with the HTS coil.

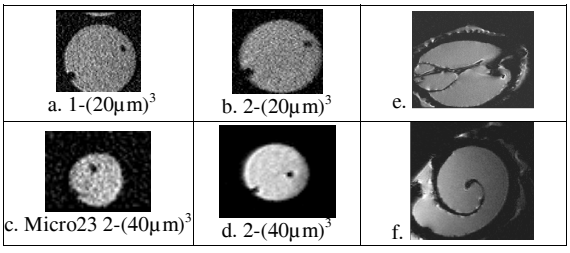


Figure1: phantom MR Images acquired with parameters described on Table 1, (a, b and d with HTS coil, c with Micro23). e and f are different view of *Trivia monacha* obtained with Protocole2-(40µm)$^3$

**Discussion and conclusion:**

To our knowledge, an acceptable SNR of 8.8 at a nominal spatial resolution of 8 pL and with realistic acquisition time (lesser than hour) has been demonstrated with a 1.5 T body scanner for the first time. The DOTA concentration in the test phantom was set to give the best possible SNR with the (20µm)$^3$ protocols according to the achieved T1 and T2 values. Using the shortest possible TE (Protocol 1) at very high spatial resolutions with the Philips Achieva scanner leads to a poor signal-averaging efficiency (SAE of 0.056) penalizing the SNR by a factor of 0.3 as compared to the one available with more powerful gradient systems but generally at the cost of a reduced access. Accounting for the signal loss relative to the long *TE* it leads to a SNR almost 2.5 times smaller than with Protocol 2. Working with small acquisition bandwidths to improve SAE may increase susceptibility artifacts and geometrical image distortion due to main field heterogeneities, as visible on the shape of the test phantom at 7 Hz/pixel. However no shimming procedure was applied in the present experiment, and the use of a relatively small field strength, compared to the ones usually employed with dedicated MR microscopes, brings a clear advantage with such artifacts. Finally, in-vivo investigations with (30µm)$^3$ acquisition is conceivable according to the observed SNR values, preferred applications being local studies on small animals or at the human body periphery (skin, joints).

[1] Zhang, Z., et al., Magma, 2004. **17**(3-6): p. 201-9, [2] Foster-Gareau et al., MRM, 2003. **49**(5): p. 968-71, [3] Ginefri et al. 2001MRM **45**, p.376-38, [4] Girard et al. 2006, 14th ISMRM, p. 222, [5] Darrasse et al. 2003, Biochimie **85**, pp.915-93